Assessing uncertainty in the dynamical ice response to ocean warming in the Amundsen Sea Embayment, West Antarctica

I. J. Nias[1,2,3], S. L. Cornford[4], T. L. Edwards[5], N. Gourmelen[6], A. J. Payne[1]

[1]Centre of Polar Observation and Modelling, School of Geographical Sciences, University of Bristol, Bristol, UK
[2]Cryospheric Sciences Laboratory, NASA Goddard Space Flight Center, Greenbelt, MD, USA
[3]Earth System Science Interdisciplinary Center, University of Maryland, College Park, MD, USA
[4]Department of Geography, Swansea University, Swansea, UK
[5]Department of Geography, Kings College London, UK
[6]School of Geosciences, University of Edinburgh, Edinburgh, UK

Key Points:

- We calibrate an ensemble of high-resolution ice-flow simulations of the Amundsen Sea Embayment, using surface elevation change observations.
- The upper tail of the distribution of sea level contribution produced by the calibrated ensemble becomes more exaggerated over time.
- Process-based modeling is essential for projecting the contribution of ice sheets to sea level.

Corresponding author: I. J. Nias, isabel.j.nias@nasa.gov

Abstract

Ice mass loss from the Amundsen Sea Embayment ice streams in West Antarctica is a major source of uncertainty in projections of future sea-level rise. Physically-based ice-flow models rely on a number of parameters that represent unobservable quantities and processes, and accounting for uncertainty in these parameters can lead to a wide range of dynamic responses. Here we perform a Bayesian calibration of a perturbed-parameter ensemble, in which we score each ensemble member on its ability to match the magnitude and broad spatial pattern of present-day observations of ice sheet surface elevation change. We apply an idealized melt-rate forcing to extend the most likely simulations forward to 2200. We find that diverging grounding-line response between ensemble members drives an exaggeration in the upper tail of the distribution of sea level rise by 2200, demonstrating that extreme future outcomes cannot be excluded.

1 Introduction

Despite considerable advances in physically-based models of ice dynamics over the last decade (Pattyn et al., 2017), there are still large uncertainties in the projections of future sea-level rise from the Antarctic ice sheets. One major focus of uncertainty is the dynamic response of fast-flowing ice streams in regions that are grounded well below sea level, in particular the Amundsen Sea Embayment (ASE). Specifically, there is uncertainty regarding the onset, speed and extent of large-scale grounding line retreat given the Marine Ice Sheet Instability theory (Favier et al., 2014; Joughin et al., 2014; Seroussi et al., 2014). Quantifying likely sea-level rise over the coming centuries is critical to the adequate provision of coastal defences.

The aim of this work is to demonstrate how spatial data of present-day observations can be used to calibrate an ensemble of ice-flow model simulations, in order to construct a probability distribution of future sea-level rise from the ASE. Quantification of uncertainty has been an integral part of global climate model projection for a number of years and features heavily in the IPCC assessment reports (Collins et al., 2013). However, only in the last few years has the ice-sheet-modelling community begun to formally consider uncertainty when estimating future contributions to sea-level (Applegate et al., 2012; Gladstone et al., 2012; Little et al., 2013; Levermann et al., 2014; Edwards et al., 2014a, 2014b, 2019; Chang et al., 2014; Ritz et al., 2015; Ruckert et al., 2017; Tsai et al., 2017; Schlegel et al., 2018). This delay is due, in part, to computational issues making it difficult to produce sufficiently large ensembles of simulations to investigate parameter uncertainty with available computational resources (Chang et al., 2014).

Several of the previous studies that do consider uncertainty focus on Greenland, where the fate of the ice sheet tends to be dependent on the modelled relationship between surface mass balance and surface elevation (Applegate et al., 2012; Edwards et al., 2014a, 2014b); ocean-driven dynamics, while under-resolved, play a less important role in the ice sheet's behavior (Fürst et al., 2015; Goelzer et al., 2018), compared with the ASE. Studies that focus on Antarctica vary in model resolution, complexity and spatial extent. Many Antarctic-wide studies use low-resolution models, which has consequences for the treatment of grounding line migration, often relying on parameterization (Levermann et al., 2014; Ritz et al., 2015; DeConto & Pollard, 2016; Edwards et al., 2019).

Depending on the magnitude of the step change in basal sliding and melt rate at the grounding line (Gladstone et al., 2017), explicitly simulating fine-scale grounding line dynamics (i.e. without relying on parameterization), requires sub-kilometer grid resolution at the grounding line (Cornford et al., 2016), which is computationally expensive. We use the BISICLES ice-flow model, which relies on adaptive mesh refinement, where the vicinity of the grounding line is modelled at a considerably higher resolution (250 m) than the interior of the ice sheet (4 km). We focus on a smaller area – the ASE, rather than the whole of Antarctica – as this region is likely to dominate the Antarctic mass loss signal in the next one to two centuries (Levermann et al., 2014; Ritz et al., 2015; DeConto & Pollard, 2016). These decisions allow us to perform a sufficient number of simulations using a sophisticated, high-resolution model to explore the likely range of dynamic response of the ASE to an idealized increase in sub-ice-shelf melting.

Firstly, we perform a Bayesian calibration of a perturbed-parameter ensemble of ice-sheet model simulations, by comparing the model results with observations of surface elevation change. We then extend the calibrated ensemble to 2200 using an idealized melt-rate forcing, and explore the uncertainty in the ice-sheet response given this forcing scenario.

2 Perturbed-parameter Ensemble Calibration

2.1 Model and Observation Data

The perturbed-parameter ensemble is described in Nias et al. (2016); here we will outline the relevant details. The BISICLES ice flow model is initialised to present-day conditions by performing an iterative procedure to find unknown quantities such as the basal traction coefficient (C), the ice viscosity stiffening factor (φ) and the sub-ice-shelf melt rate (M_b) (Nias et al., 2016). C and φ are found by solving an inverse problem given observations of velocity (Rignot et al., 2011). M_b is determined from the flux divergence over floating ice, but is parameterized to be spatially smooth and to have the highest rates close to the grounding line. Two alternative initial states are created; one that uses the Bedmap2 geometry (Fretwell et al., 2013), and one that modifies the bed topography and grounded ice thickness to smooth spurious thickening signals in the flux divergence, which have been attributed to incorrect thickness measurements (Morlighem et al., 2011; Nias et al., 2018).

In total there are four optimal parameter sets, for all combinations of the two bedrock geometries and two Weertman sliding laws ($m = 1$ and $m = 1/3$), which form the basis of the ensemble. Nias et al. (2016) use Latin hypercube sampling to create 64 distinct parameter vectors in which C, φ and M_b vary between a halving and a doubling of the optimised values, which, with the addition of the optimal member and six end members, produces a 284-member ensemble. The 50-year simulations are run under present conditions, i.e. there is no time-dependent climate forcing.

Observed rates of surface elevation change ($\mathrm{d}h/\mathrm{d}t$) over grounded ice are obtained from swath processing of CryoSat-2 radar altimetry measurements from 2010 to 2015 (Gourmelen et al., 2017). This processing technique is able to capture thinning rates in the swath rather than just the Point Of Closest Approach (POCA). In doing so it provides a greater spatial coverage of $\mathrm{d}h/\mathrm{d}t$ measurements compared to traditional POCA technique (Foresta et al., 2016). The spatial resolution of the data is approximately 500 m.

2.2 Bayesian Calibration

Bayes' theorem states that the posterior probability distribution ($P(\theta|Y)$ – the probability of θ given Y) is proportional to the prior probability distribution ($P(\theta)$ – the probability of θ) multiplied by a likelihood function ($P(Y|\theta)$ – probability of Y given θ):

$$P(\theta|Y) \propto P(\theta)P(Y|\theta)\,. \tag{1}$$

In other words, we are trying to find the probability of an event (e.g. a magnitude of sea level rise) produced by a particular parameter vector θ (e.g. the scaling factors used to vary C, φ and M_b), given observations Y (e.g. $\mathrm{d}h/\mathrm{d}t$). We are not trying to find a single estimate of θ, rather a distribution.

Each ensemble member is assigned a likelihood score based on discrepancies between the model output and observed $\mathrm{d}h/\mathrm{d}t$, assuming Gaussian, independent errors (Edwards et al., 2014b). The likelihood score s_j for the j^{th} simulation in the ensemble is

$$s_j = \exp\left[-\frac{1}{2}\sum_i \frac{(f_i^j - z_i^j)^2}{(\sigma_i^j)^2}\right], \tag{2}$$

where f is the modelled $\mathrm{d}h/\mathrm{d}t$ and z is the observed $\mathrm{d}h/\mathrm{d}t$, and i is a spatial index.

σ^2 is the discrepancy variance, which is a combination of observational error and structural error, and represents the mismatch between the model, given the optimum parameter set, and the real world (Murphy et al., 2009; Edwards et al., 2019). Observational error is found from the covariance matrix of the parameters used to derive the swath-processed $\mathrm{d}h/\mathrm{d}t$ (Foresta et al., 2016). Structural error has numerous sources related to the structural properties of the model; for example missed physical processes, spatial resolution of the grid and the numerical representation. Structural error is poorly constrained and so we conservatively assign it a value of double the observational error (Fig. S4).

Often in model-data evaluation, spatial comparisons are made at every available location. While this is appealing in terms of maximising the number of data points, the spatial correlation inherent in most environmental variables means that this tends to overly penalise models in regions of coherent spatial patterns. The model error is 'double-counted' for each neighbouring grid cell, even though they arise from a common source. One approach is to model this spatial correlation explicitly, but this is challenging and requires assumptions about the precise features of grid cell-to-cell correlations everywhere. A more common approach is to remove the spatial correlation by averaging or sub-sampling the data at a spatial scale at which they are reduced so the model-data discrepancies are sufficiently independent.

Using semi-variograms, we empirically investigate the length scales at which the covariance is reduced to an acceptable value, and use this to decide upon an appropriate spatial scale on which to sample the discrepancies. We find this to be approximately 100 km, both in the x- and y-directions (see the Supporting Information).

The score for each simulation is normalised to create a weight w,

$$w_j = \frac{s_j}{\sum_j s_j}, \tag{3}$$

where the simulation with the lowest discrepancy with observations has the largest weight. These weights, which are akin to $P(Y|\theta)$ in Equation 1, are used to weight the prior distribution, $P(\theta)$, to produce a calibrated (posterior) distribution of sea level contribution, $P(\theta|Y)$ (Fig. 1a).

The most likely (modal) sea-level rise estimate according to the prior distribution is 0.26 mm yr^{-1} (50-year mean), which shifts to 0.30 mm yr^{-1} in the posterior distribution (Table 1). The similarity between these estimates and observed rates of mass loss from the ASE (Fig. 1a), indicates that these independent methods for quantifying present-day mass loss are in good agreement; whether it is BISICLES tuned using velocity observations (the prior); the observed spatial field of surface elevation change (the posterior); or the methods used to estimate total mass loss from the ice sheet (vertical lines, Fig. 1a). The spread of the posterior distribution is reduced from the prior distribution, indicating that the calibration process is useful for reducing uncertainty in sea level rise projections. Future work could test the impact of using different types of observational data in the calibration process. For example, maps of observed velocity change could be a good candidate, as the dynamic signal is not influenced by changes in surface mass balance.

Table 1. Quantiles and modes for the prior and posterior distributions of the 50-year mean rate of sea-level contribution (mm yr^{-1}); and cumulative sea level total (mm) after 100 and 200 years with increased melt forcing.

		5%	25%	50%	75%	95%	Mode
Rates	Prior	-0.08	0.14	0.35	0.67	1.35	0.26
(mm yr^{-1})	Posterior	0.02	0.19	0.33	0.46	0.72	0.30
Total	100 years	20.6	38.3	55.7	72.2	123.1	53.7
(mm)	200 years	56.2	106.9	139.7	239.9	424.3	119.6

3 Extended Simulations

Of the 284-member ensemble, 187 members were within the 5–95% probability interval of the 50-year mean rate of sea-level contribution (0.02-0.72 mm yr^{-1}, Table 1). We exclude the extremes because their implied rates of elevation change perform poorly in the comparison with present-day observations (at the 10% probability level). Satellite observations have consistently shown that the ASE has been losing mass (Mouginot et al., 2014; McMillan et al., 2014), and so it is particularly appropriate to discard those members with mass gain. In addition, previous regional modelling has suggested that a linear-viscous law is not suitable for describing sliding over bedrock and is prone to underestimate the sensitivity to changes in basal traction at the grounding line (Joughin et al., 2009, 2010). Therefore, given limited computational resources, we chose to extend to 2200 only the 71 ensemble members that fall within the 5–95% probability interval of sea-level contribution and use the non-linear ($m = 1/3$) Weertman sliding law.

The sub-ice-shelf melt-rate is perturbed within the perturbed-parameter ensemble described above. In addition, we apply a simplified melt-rate forcing anomaly to ensure the direction of change is consistent with the expected behaviour. In the Amundsen Sea, we expect there to be an increase in sub-ice-shelf melt-rates over the coming centuries due to increasing Circumpolar Deep Water (CDW) intrusions onto the continental shelf, as well as potentially direct warming (Timmermann & Hellmer, 2013; Holland et al., 2019). Therefore, we apply an idealized melt-rate forcing, based loosely on regional ocean modelling, given a 'business-as-usual' emissions scenario (Timmermann et al., 2002). The ice-shelf averaged melt-rate anomaly increases linearly to 15 m yr^{-1} by the end of the 21$^{\text{st}}$ century – as ice shelf contact with the CDW increases – and remains constantly elevated in the 22$^{\text{nd}}$ century – representing continued CDW intrusion. The mean melt-rate anomaly is in addition to the melt rates of the perturbed-parameter ensemble ($\sim$5–20 m yr^{-1} mean), and is distributed to be highest near to the grounding line. Further details about the melt-rate forcing can be found in the Supporting Information.

All the extended simulations continued to lose mass from the ASE, and by the end of the two centuries the modal contribution is 12 cm sea level equivalent (Table 1). The probability distributions of cumulative sea-level contribution (Fig. 1b) broaden over time, particularly in the upper tail of the distribution where the contribution in the second century is larger than in the first. This super-linear response persists, even when the melt rate remains constant in the second century. However, other simulations maintain an approximately linear response at a lower rate throughout the 200-year simulations. These two response types can be seen in Figure 2c; approximately 40% of the simulations exhibit a super-linear trend (blue lines).

By the end of the 21$^{\text{st}}$ century, all ensemble members have experienced a reduction in the total ASE grounded area (Fig. 2a). However, retreat is not ubiquitous across all ice streams: some members result in grounding line advance, albeit limited, in Pine

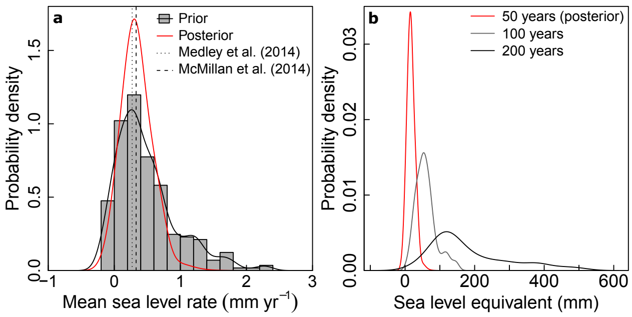

Figure 1. Distributions of sea level change. a) Histogram (grey boxes) and associated prior probability density function (prior PDF, black curve) of present-day sea-level contribution rate (50 year mean) from the original model ensemble, and calibrated posterior PDF (red curve). Observed rates from 2010 using the input-output method (0.27 ± 0.04 mm yr^{-1}, short dashes) (Medley et al., 2014) and 2010–2013 derived from Cryosat-2 altimetry (0.33 ± 0.05 mm yr^{-1}, long dashes) (McMillan et al., 2014) are represented by vertical lines. b) PDFs of the total sea-level contribution from the calibrated 50-year ensemble (red curve); and from the extended ensemble after 100 years (grey curve) and 200 years (black curve).

Island and Thwaites glaciers. The group of smaller ice streams to the west of Thwaites (Pope, Smith, Kohler glaciers – PSK) do show grounding line retreat in all ensemble members.

4 Discussion

During the 200-year simulations, the high-end ensemble members diverge from the modal behavior, creating a skewed distribution towards higher values of sea level contribution (Fig. 1b). This is despite the high-end tail of the original ensemble being down-weighted (Fig. 1a), resulting in the most extreme simulations being removed from the longer century-scale simulations. Non-normal distributions, characterized by a long tail at the high end, are also found in other studies (Levermann et al., 2014; DeConto & Pollard, 2016; Kopp et al., 2017; Edwards et al., 2019; Robel et al., 2019).

The super-linear response of the high-end members means that while the mode of the distribution increases linearly – the total sea level contribution after 200 years is approximately double the total after 100 years – the 95$^{\text{th}}$ percentile increases disproportionately (Table 1). Given our idealized melt-rate forcing, there is 5% probability that the ASE will contribute more than 12 cm of sea level rise by $\sim$2100 and 42 cm by $\sim$2200. This is in contrast to a study by Ritz et al. (2015), in which the response at the 95$^{\text{th}}$ percentile is quasi-linear, with 25 cm of sea level rise from the ASE in the 21st century and 48 cm by 2200. In their model, the representation of ice dynamics is simpler and at a lower resolution (15 km) than the model used here. In particular, the grounding line retreat is imposed rather than computed, which may dampen non-linear behaviour.

We find that the grounding line behavior regulates the linearity of the sea-level response. Indeed, the long tail at the high end of the sea-level rise distribution is mirrored in the grounding line retreat: some simulations achieve extreme retreat, whereas many simulations experience more modest retreat and advance is limited (Fig. 2). As the ice stream grounding lines retreat further into the deep basins they inhabit, the flux across them increases with ice thickness and with the lengthening of the flux-gate. The rela-

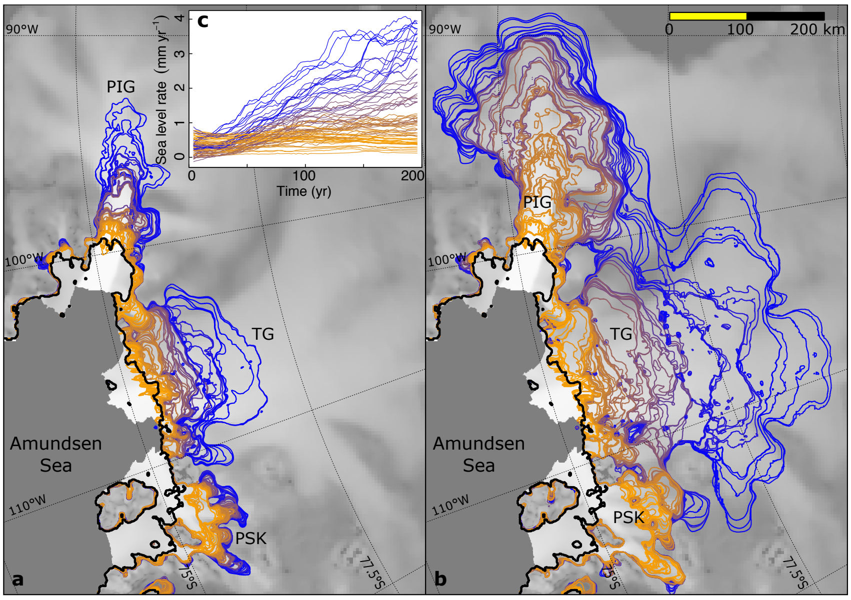

Figure 2. Grounding line position after a) 100 years and b) 200 years. Each coloured line represents an individual ensemble member: yellow represents a more linear sea-level response and blue represents a super-linear response (based on the second derivative of the sea level trend shown in c) the 8-year running-mean of the rate of sea-level contribution from the ASE during the 200-year simulations). The initial grounding line position is delineated by the thick black line. Grey scale background indicates initial velocity.

tionship between grounding line retreat and the non-linearity of the sea level response over time is illustrated by the colored lines in Figure 2.

As alluded to above, the non-linearity in the rate of grounding line retreat is related to the bedrock topography, as demonstrated for Pine Island Glacier in Figure 3. Approximately 18% of our simulations maintain their initial grounding line position (in the case of the Bedmap2 simulations), or close to it (in the case of the modified bedrock, which has a topographic rise ∼15 km upstream) for much, if not all, of the simulations. Others experience only limited retreat, with a number of topographic rises, most notably at ∼25 km upstream of the initial grounding line position, producing a step-like pattern in retreat (Fig. 3). These modest responses are similar to the first mode of retreat described by Gladstone et al. (2012), in which retreat is gradual on the order of 0.1 km yr^{-1}.

Gladstone et al. (2012) find a second mode of grounding line behavior characterized by rapid accelerating retreat. In their flow-line model simulations the initial grounding line retreat off the bedrock high occurs quickly and, once it reaches an uninterrupted retrograde slope, the rate of retreat can reach up to 10 km yr^{-1} and be sustained for up to ∼10 years, which is similar to our most extreme results (Fig. 3). The similarities between our results and those shown in Figure 3 of Gladstone et al. (2012), despite the significant differences in model physics, indicates that topography, as well as the forcing, exerts a strong control on the temporal form of Pine Island Glacier grounding line retreat.

Robel et al. (2019) demonstrate that an ensemble becomes progressively more skewed towards greater retreat when the grounding line is located on a predominantly retrograde bedrock slope, because the rate of retreat in the extreme ensemble members diverges further away from the more moderate members – which is seen here in Figure 3. The skew-

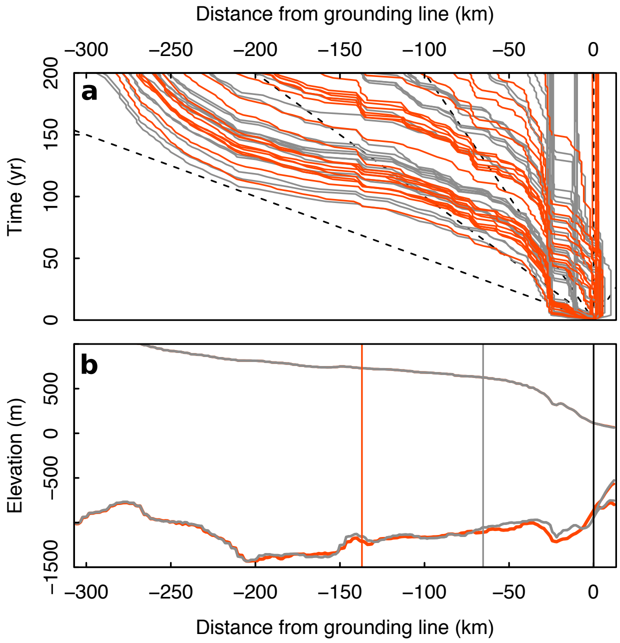

Figure 3. Pine Island Glacier a) grounding line retreat over time, relative to the initial position (0 km), with each curve representing one simulation. Dashed lines act as a guide for linear retreat rates. b) cross-section of the two geometries: Bedmap2 (Fretwell et al., 2013) (orange) and the modified bed (Nias et al., 2016) (grey). The top lines represent the initial ice surface, and the bottom lines gives the bed topography. To the right of 0 km (initial grounding line – black line), the bed topography diverges from the ice base (i.e. the ice shelf). The colored vertical lines are at the position of the grounding line of the central ensemble members after 200 years, for the two geometries.

ness in the distribution towards the high-end of sea level rise is fundamentally linked to the non-linearity in the rate of grounding line retreat (Robel et al., 2019).

Missed processes in the model contribute to its structural error. For example, we do not include calving in our model – the ice front is fixed and we impose a minimum ice thickness of 10 m. This could have implications for stability as ice shelves can provide a buttressing effect on the grounded ice sheet (Gudmundsson, 2013); although in many cases here the simulated ice shelf, across the vast majority of the area, is close to or at the minimum thickness constraint of 10 m, the buttressing effect of which is negligible. The lack of calving and ice shelf collapse, precludes any potential loss through marine ice cliff instability (DeConto & Pollard, 2016), although on the timescales of this study, it is unlikely that sufficient surface melt will occur to cause ice shelf collapse in the ASE (Trusel et al., 2015; Kuipers Munneke et al., 2014). Another source of model uncertainty is the sliding law used to determine basal shear stress – the choice of which can lead to different ice sheet responses (Brondex et al., 2017, 2019; Nias et al., 2018). Given the amount of grounding line retreat experienced by the extreme simulations, we would expect interactions with neighboring West Antarctic drainage basins (Feldmann & Levermann, 2015; Cornford et al., 2016). However our model configuration has a fixed boundary so these dynamics have not been explored here.

Ocean-driven melt is likely to be a major source of uncertainty in future projections of sea level rise (Schlegel et al., 2018; Nowicki & Seroussi, 2018), for example there is uncertainty in the future ocean temperature projection, and its relationship to melt rate, and how this is parameterized in BISICLES. Here, we have tested the impact of uncertainty in the melt rate obtained during the initialization of BISICLES: halving and doubling the optimal melt-rate field results in a 4 cm difference in sea level contribution by 2200, when all other parameters are held at their optimal values. This is an order of magnitude less than the total spread of the distribution given in Table 1. However, we have not investigated the impact of uncertainty in the melt-rate forcing anomaly added during the extended simulations. Accounting for different ocean temperature projections is likely to add considerable spread to the distribution of future sea level contribution (Holland et al., 2019), whereas the precise form of the ocean melt parameterization is likely to be less influential (Favier et al., 2019).

For the PSK group of ice streams, retreat occurs in all ensemble members and there is less ambiguity in the future outlook, compared with Pine Island and Thwaites glaciers (Fig. 2). Smith Glacier in particular has seen rapid retreat over the last two decades, and although there has been a recent slow-down in the retreat, Scheuchl et al. (2016) predict that it will continue unabated in the coming years, and they have attributed the recent stabilization to a locally prograde slope. The uncertainty in future sea-level rise from the ASE lies in the vast range of responses exhibited in Pine Island and Thwaites glaciers, not the PSK group, which are relatively consistent with one another and where the potential for retreat is much more limited by the topographic constraints.

Simulations that behave similarly at the beginning of the 200 year simulations do not necessarily follow a similar trajectory (Fig. S5). This demonstrates that it is essential to use process-based models, which can predict the changing evolution of the ice sheet, instead of extrapolation methods when making projections; as also found by others (Ritz et al., 2015; Kopp et al., 2017).

5 Conclusion

Here we have attempted to constrain and quantify the uncertainty in sea level rise from the ASE using BISICLES, a high-resolution ice-flow model capable of capturing grounding line dynamics. Using present-day (2010–2015) observations we calibrated the perturbed-parameter ensemble of Nias et al. (2016), by scoring each member on its ability to match the magnitude and spatial pattern of surface elevation change. Based on the resulting posterior distribution of sea-level change rates, the extreme ensemble members, which matched poorly with observations, were discarded. Simulations that start out in agreement with the present day can end up contributing more than 42 cm (5% probability) by 2200, although the modal estimate is 12 cm. The long high-end tail of the sea-level distribution becomes more exaggerated over time due to extreme members exhibiting a super-linear sea-level response, and is mirrored in the divergence in grounding-line response between ensemble members. Our results only reflect uncertainty in the ice dynamics, and the range of potential outcomes would be greater if the uncertainty in the projected forcing is also included. Overall the uncertainty in the response of this particularly dynamic region of Antarctica is a major challenge in provisions for mitigating the impact of sea-level rise, and at this time extreme future outcomes cannot be excluded.

Acknowledgments

This work was supported by funding from the UK Natural Environment Research Council (NERC) through the iSTAR-C programme (NE/J005738/1). NG was supported by European Space Agency contract CryoTop Evolution 4000116874/16/I-NB. BISICLES simulations were performed on the University of Bristol's Blue Crystal Phase 3 supercomputer. Code used to configure the BISICLES ensemble is available at https://github.com/ijnias/nias-et-al-2019-grl. The model output is in long-term storage in the University of Bristol Research Data Storage Facility and is available on request. We thank the editor, Mathieu Morlighem, and reviewers for their comments on the manuscript.

References

Applegate, P. J., Kirchner, N., Stone, E. J., Keller, K., & Greve, R. (2012). An assessment of key model parametric uncertainties in projections of Greenland Ice Sheet behavior. *The Cryosphere*, *6*(3), 589–606. doi: 10.5194/tc-6-589-2012

Brondex, J., Gagliardini, O., Gillet-Chaulet, F., & Durand, G. (2017). Sensitivity of grounding line dynamics to the choice of the friction law. *Journal of Glaciology*, *63*(241), 854–866. doi: 10.1017/jog.2017.51

Brondex, J., Gillet-Chaulet, F., & Gagliardini, O. (2019). Sensitivity of centennial mass loss projections of the Amundsen basin to the friction law. *The Cryosphere*, *13*(1), 177–195. doi: 10.5194/tc-13-177-2019

Chang, W., Applegate, P. J., Haran, M., & Keller, K. (2014). Probabilistic calibration of a Greenland Ice Sheet model using spatially resolved synthetic observations: toward projections of ice mass loss with uncertainties. *Geoscientific Model Development*, *7*(5), 1933–1943. doi: 10.5194/gmd-7-1933-2014

Collins, M., Knutti, R., Arblaster, J., Dufresne, J.-L., Fichefet, T., Friedlingstein, P., … Wehner, M. (2013). Long-term Climate Change: Projections, Commitments and Irreversibility. In T. Stocker et al. (Eds.), *Climate Change 2013: The Physical Science Basis. Contribution of Working Group I to the Fifth Assessment Report of the Intergovernmental Panel on Climate Change* (pp. 1029–1136). Cambridge, United Kingdom and New York, NY, USA: Cambridge University Press. Retrieved from `www.climatechange2013.org`

Cornford, S. L., Martin, D. F., Lee, V., Payne, A. J., & Ng, E. G. (2016). Adaptive mesh refinement versus subgrid friction interpolation in simulations of Antarctic ice dynamics. *Annals of Glaciology*, 1–9. doi: 10.1017/aog.2016.13

DeConto, R. M., & Pollard, D. (2016). Contribution of Antarctica to past and future sea-level rise. *Nature*, *531*(7596), 591–597. doi: 10.1038/nature17145

Edwards, T. L., Brandon, M. A., Durand, G., Edwards, N. R., Golledge, N. R., Holden, P. B., … Wernecke, A. (2019). Revisiting Antarctic ice loss due to marine ice-cliff instability. *Nature*, *566*(7742), 58–64. doi: 10.1038/s41586-019-0901-4

Edwards, T. L., Fettweis, X., Gagliardini, O., Gillet-Chaulet, F., Goelzer, H., Gregory, J. M., … Ritz, C. (2014a). Effect of uncertainty in surface mass balanceelevation feedback on projections of the future sea level contribution of the Greenland ice sheet. *The Cryosphere*, *8*(1), 195–208. doi: 10.5194/tc-8-195-2014

Edwards, T. L., Fettweis, X., Gagliardini, O., Gillet-Chaulet, F., Goelzer, H., Gregory, J. M., … Ritz, C. (2014b). Probabilistic parameterisation of the surface mass balanceelevation feedback in regional climate model simulations of the Greenland ice sheet. *The Cryosphere*, *8*(1), 181–194. doi: 10.5194/tc-8-181-2014

Favier, L., Durand, G., Cornford, S. L., Gudmundsson, G. H., Gagliardini, O., Gillet-Chaulet, F., … Le Brocq, A. M. (2014). Retreat of Pine Island Glacier controlled by marine ice-sheet instability. *Nature Climate Change*, 1758–6798. doi: 10.1038/nclimate2094

Favier, L., Jourdain, N. C., Jenkins, A., Merino, N., Durand, G., Gagliardini, O., … Mathiot, P. (2019). Assessment of sub-shelf melting parameterisations using the oceanice-sheet coupled model NEMO(v3.6)Elmer/Ice(v8.3). *Geoscientific Model Development*, *12*(6), 2255–2283. doi: 10.5194/gmd-12-2255-2019

Feldmann, J., & Levermann, A. (2015). Interaction of marine ice-sheet instabilities in two drainage basins: simple scaling of geometry and transition time. *The Cryosphere*, *9*(2), 631–645. doi: 10.5194/tc-9-631-2015

Foresta, L., Gourmelen, N., Plsson, F., Nienow, P., Bjrnsson, H., & Shepherd, A. (2016). Surface elevation change and mass balance of Icelandic ice caps derived from swath mode CryoSat-2 altimetry. *Geophysical Research Letters*, *43*(23), 12,138–12,145. doi: 10.1002/2016GL071485

Fretwell, P., Pritchard, H. D., Vaughan, D. G., Bamber, J. L., Barrand, N. E., Bell, R., … Zirizzotti, A. (2013). Bedmap2: improved ice bed, surface and thickness datasets for Antarctica. *The Cryosphere*, *7*, 375–393. doi: 10.5194/tc-7-375-2013

Fürst, J. J., Goelzer, H., & Huybrechts, P. (2015). Ice-dynamic projections of the Greenland ice sheet in response to atmospheric and oceanic warming. *The Cryosphere*, *9*(3), 1039–1062. doi: 10.5194/tc-9-1039-2015

Gladstone, R. M., Lee, V., Rougier, J., Payne, A. J., Hellmer, H., Le Brocq, A., … Cornford, S. L. (2012). Calibrated prediction of Pine Island Glacier retreat during the 21st and 22nd centuries with a coupled flowline model. *Earth and Planetary Science Letters*, *333-334*, 191–199. doi: 10.1016/j.epsl.2012.04.022

Gladstone, R. M., Warner, R. C., Galton-Fenzi, B. K., Gagliardini, O., Zwinger, T., & Greve, R. (2017). Marine ice sheet model performance depends on basal sliding physics and sub-shelf melting. *The Cryosphere*, *11*(1), 319–329. doi: 10.5194/tc-11-319-2017

Goelzer, H., Nowicki, S., Edwards, T., Beckley, M., Abe-Ouchi, A., Aschwanden, A., … Ziemen, F. A. (2018). Design and results of the ice sheet model initialisation experiments initMIP-Greenland: an ISMIP6 intercomparison. *The Cryosphere*, *12*(4), 1433–1460. doi: 10.5194/tc-12-1433-2018

Gourmelen, N., Escorihuela, M., Shepherd, A., Foresta, L., Muir, A., Garcia-Mondejar, A., … Drinkwater, M. (2017). CryoSat-2 swath interferometric altimetry for mapping ice elevation and elevation change. *Advances in Space Research*. doi: 10.1016/j.asr.2017.11.014

Gudmundsson, G. H. (2013). Ice-shelf buttressing and the stability of marine ice sheets. *The Cryosphere*, *7*(2), 647–655. doi: 10.5194/tc-7-647-2013

Holland, P. R., Bracegirdle, T. J., Dutrieux, P., Jenkins, A., & Steig, E. J. (2019). West Antarctic ice loss influenced by internal climate variability and anthropogenic forcing. *Nature Geoscience*, *12*(9), 718–724. doi: 10.1038/s41561-019-0420-9

Joughin, I., Smith, B., & Holland, D. (2010). Sensitivity of 21st century sea level to ocean-induced thinning of Pine Island Glacier, Antarctica. *Geophysical Research Letters*, *37*, L20502. doi: 10.1029/2010gl044819

Joughin, I., Smith, B. E., & Medley, B. (2014). Marine Ice Sheet Collapse Potentially Under Way for the Thwaites Glacier Basin, West Antarctica. *Science*, *344*, 735–738. doi: 10.1126/science.1249055

Joughin, I., Tulaczyk, S., Bamber, J. L., Blankenship, D., Holt, J. W., Scambos, T., & Vaughan, D. G. (2009). Basal conditions for Pine Island and Thwaites Glaciers, West Antarctica, determined using satellite and airborne data. *Journal of Glaciology*, *55*, 245–257. doi: 10.3189/002214309788608705

Kopp, R. E., DeConto, R. M., Bader, D. A., Hay, C. C., Horton, R. M., Kulp, S., … Strauss, B. H. (2017). Evolving Understanding of Antarctic Ice-Sheet Physics and Ambiguity in Probabilistic Sea-Level Projections. *Earth's Future*, *5*(12), 1217–1233. doi: 10.1002/2017EF000663

Kuipers Munneke, P., Ligtenberg, S. R. M., Van Den Broeke, M. R., & Vaughan, D. G. (2014). Firn air depletion as a precursor of Antarctic ice-shelf collapse. *Journal of Glaciology*, *60*, 205–214. doi: 10.3189/2014JoG13J183

Levermann, A., Winkelmann, R., Nowicki, S., Fastook, J. L., Frieler, K., Greve, R., … Bindschadler, R. A. (2014). Projecting Antarctic ice discharge using response functions from SeaRISE ice-sheet models. *Earth System Dynamics*, *5*(2), 271–293. doi: 10.5194/esd-5-271-2014

Little, C. M., Oppenheimer, M., & Urban, N. M. (2013). Upper bounds on twenty-first-century Antarctic ice loss assessed using a probabilistic framework. *Nature Climate Change*, *3*(7), 654–659. doi: 10.1038/nclimate1845

McMillan, M., Shepherd, A., Sundal, A., Briggs, K., Muir, A., Ridout, A., … Wingham, D. (2014). Increased ice losses from Antarctica detected by CryoSat-2.

Geophysical Research Letters, *41*, 3899–3905. doi: 10.1002/2014GL060111
Medley, B., Joughin, I., Smith, B. E., Das, S. B., Steig, E. J., Conway, H., ... Leuschen, C. (2014). Constraining the recent mass balance of Pine Island and Thwaites glaciers, West Antarctica, with airborne observations of snow accumulation. *The Cryosphere*, *8*(4), 1375–1392. doi: 10.5194/tc-8-1375-2014
Morlighem, M., Rignot, E., Seroussi, H., Larour, E., Dhia, H. B., & Aubry, D. (2011). A mass conservation approach for mapping glacier ice thickness. *Geophysical Research Letters*, *38*. doi: 10.1029/2011GL048659
Mouginot, J., Rignot, E., & Scheuchl, B. (2014). Sustained increase in ice discharge from the Amundsen Sea Embayment, West Antarctica, from 1973 to 2013. *Geophysical Research Letters*, *41*, 1576–1584. doi: 10.1002/2013gl059069
Murphy, J., Sexton, D., Jenkins, G., Boorman, P., Booth, B., Brown, C., ... Wood, R. (2009). *UK Climate Projections Science Report: Climate change projections.* Exeter: Met Office Hadley Centre. Retrieved 2017-05-29, from `http://ukclimateprojections.defra.gov.uk/content/view/824/517/index.html`
Nias, I. J., Cornford, S. L., & Payne, A. J. (2016). Contrasting the modelled sensitivity of the Amundsen Sea Embayment ice streams. *Journal of Glaciology*, *62*(233), 552–562. doi: 10.1017/jog.2016.40
Nias, I. J., Cornford, S. L., & Payne, A. J. (2018). New mass-conserving bedrock topography for Pine Island Glacier impacts simulated decadal rates of mass loss. *Geophysical Research Letters*, *45*(7), 3173–3181. doi: 10.1002/2017GL076493
Nowicki, S., & Seroussi, H. (2018). Projections of Future Sea Level Contributions from the Greenland and Antarctic Ice Sheets: Challenges Beyond Dynamical Ice Sheet Modeling. *Oceanography*, *31*(2). doi: 10.5670/oceanog.2018.216
Pattyn, F., Favier, L., Sun, S., & Durand, G. (2017). Progress in Numerical Modeling of Antarctic Ice-Sheet Dynamics. *Current Climate Change Reports*, *3*(3), 174–184. doi: 10.1007/s40641-017-0069-7
Rignot, E., Mouginot, J., & Scheuchl, B. (2011). Ice flow of the Antarctic ice sheet. *Science*, *333*, 1427–1430. doi: 10.1126/science.1208336
Ritz, C., Edwards, T. L., Durand, G., Payne, A. J., Peyaud, V., & Hindmarsh, R. C. A. (2015). Potential sea-level rise from Antarctic ice-sheet instability constrained by observations. *Nature*, *528*(7580), 115–118. doi: 10.1038/nature16147
Robel, A. A., Seroussi, H., & Roe, G. H. (2019). Marine ice sheet instability amplifies and skews uncertainty in projections of future sea-level rise. *Proceedings of the National Academy of Sciences*, *116*(30), 14887–14892. doi: 10.1073/pnas.1904822116
Ruckert, K. L., Shaffer, G., Pollard, D., Guan, Y., Wong, T. E., Forest, C. E., & Keller, K. (2017). Assessing the Impact of Retreat Mechanisms in a Simple Antarctic Ice Sheet Model Using Bayesian Calibration. *PLOS ONE*, *12*(1), e0170052. doi: 10.1371/journal.pone.0170052
Scheuchl, B., Mouginot, J., Rignot, E., Morlighem, M., & Khazendar, A. (2016). Grounding line retreat of Pope, Smith, and Kohler Glaciers, West Antarctica, measured with Sentinel-1a radar interferometry data. *Geophysical Research Letters*, *43*(16), 2016GL069287. doi: 10.1002/2016GL069287
Schlegel, N.-J., Seroussi, H., Schodlok, M. P., Larour, E. Y., Boening, C., Limonadi, D., ... van den Broeke, M. R. (2018). Exploration of Antarctic Ice Sheet 100-year contribution to sea level rise and associated model uncertainties using the ISSM framework. *The Cryosphere*, *12*(11), 3511–3534. doi: 10.5194/tc-12-3511-2018
Seroussi, H., Morlighem, M., Rignot, E., Mouginot, J., Larour, E., Schodlok, M., & Khazendar, A. (2014). Sensitivity of the dynamics of Pine Island Glacier, West Antarctica, to climate forcing for the next 50 years. *The Cryosphere*, *8*(5), 1699–1710. doi: 10.5194/tc-8-1699-2014
Timmermann, R., Beckmann, A., & Hellmer, H. H. (2002). Simulations of ice-ocean

dynamics in the Weddell Sea 1. Model configuration and validation. *Journal of Geophysical Research*, *107*(C3). doi: 10.1029/2000JC000741

Timmermann, R., & Hellmer, H. H. (2013). Southern Ocean warming and increased ice shelf basal melting in the twenty-first and twenty-second centuries based on coupled ice-ocean finite-element modelling. *Ocean Dynamics*, *63*(9-10), 1011–1026. doi: 10.1007/s10236-013-0642-0

Trusel, L. D., Frey, K. E., Das, S. B., Karnauskas, K. B., Kuipers Munneke, P., van Meijgaard, E., & van den Broeke, M. R. (2015). Divergent trajectories of Antarctic surface melt under two twenty-first-century climate scenarios. *Nature Geoscience*, *8*(12), 927–932. doi: 10.1038/ngeo2563

Tsai, C.-Y., Forest, C. E., & Pollard, D. (2017). Assessing the contribution of internal climate variability to anthropogenic changes in ice sheet volume. *Geophysical Research Letters*, *44*(12), 6261–6268. doi: 10.1002/2017GL073443